Heliyon 9 (2023) e18352

Contents lists available at ScienceDirect

Heliyon

journal homepage: www.cell.com/heliyon

Insight into the effect of chemical structure for microbial lignite methanation

Lin Yang [a,b,c], Yongfeng Zhang [a,b,c,*], Zhifei Hao [a,b,c], Junying Zhang [d,**]

[a] College of Chemical Engineering, Inner Mongolia University of Technology, Hohhot, 010051, China
[b] Inner Mongolia Key Laboratory of Efficient Cyclic Utilization of Coal-Based Solid Waste, Hohhot, 010051, China
[c] Key Laboratory of Resource Circulation at Universities of Inner Mongolia Autonomous Region, Hohhot, 010051, China
[d] State Key Laboratory of Coal Combustion, Huazhong University of Science and Technology, Wuhan, 430074, China

ARTICLE INFO

Keywords:
Lignite
Biodegradation
Chemical structure
Crushing pretreatment
Ball milling pretreatment

ABSTRACT

The chemical structure of lignite plays a fundamental role in microbial degradation, which can be altered to increase gas production. In this study, the structural changes in lignite were analyzed by conducting pretreatment and biomethane gas production experiments using crushing and ball milling processes, respectively. The results revealed that different particle size ranges of lignite considerably influence gas production. The maximum methane yield under both treatments corresponded to a particle size range of 400–500 mesh. The gas production after ball milling was higher than that after crushing, irrespective of particle size. Compared with lignite subjected to crushing, that subjected to ball milling exhibited more oxygen-containing functional groups, less coalification, more disordered structures, and small aromatic ring structures, demonstrating more unstable properties, which are typically favorable to microbial flora for the utilization and degradation of lignite. Additionally, a symbiotic microbial community comprising multiple species was established during the microbial degradation of lignite into biogas. This study provides new insights and a strong scientific foundation for further research on microbial lignite methanation.

1. Introduction

Coal biogasification is a crucial step towards achieving the goals of clean use, energy savings, and emission reductions from coal [1]. It is the focus of microbial enhanced coal bed methane (MECBM) mining. With the development and utilization of coal bed methane (CBM) resources, a deeper understanding of biogenic CBM has been gained. Many scholars have successfully simulated biogas generation in coal seam under laboratory conditions [2–4].

Scott proposed the concept of bio-enhanced CBM production for biogasification [5]. The microbial flora obtained from abandoned coal mines can be introduced into a refractory coal-containing matrix, which can then be degraded into methane and carbon dioxide gases under appropriate conditions [6,7]. The methane produced during coal biogasification provides a safe, efficient, and inexpensive source of energy. Research on anaerobic microbial degradation of subbituminous coal [8] demonstrates that organic intermediates related to gas production mainly include long-chain fatty acids, alkanes, and various low-molecular weight aromatic hydrocarbons

* Corresponding author. College of Chemical Engineering, Inner Mongolia University of Technology, Hohhot, 010051, China.
** Corresponding author.
E-mail addresses: environzyf@sina.com (Y. Zhang), jyzhang@hust.edu.cn (J. Zhang).

https://doi.org/10.1016/j.heliyon.2023.e18352
Received 22 May 2023; Received in revised form 6 July 2023; Accepted 13 July 2023
Available online 16 July 2023

(including phenols) [9]. Methanogenic flora obtained from subsurface reservoirs can produce methane from more than 30 types of methoxyl aromatic compounds [10] through oxygen demethylation, carbon dioxide reduction, and acetyl-CoA metabolism. Physical, chemical, and biological measures can be used to increase biological methane production by promoting the hydrolysis of organic materials in coal [11,12]. The small molecular organic matter in coal, particularly in low-rank coal, is readily degraded by bacteria [13–15]. The hydrolysis of coal to soluble organic intermediates is the limiting step for the conversion of coal to biomethane [1,16].

To date, efforts have been made in the biodegradation of lignite, although mostly from the perspective of microbial flora [17,18]; however, the impact of the structure of lignite on biodegradation has rarely been studied. There have been studies of the biological gas production after simulated lignite pretreatment, revealing subsequent increase in gas production following pretreatment [12,19,20]. However, there are still some gaps in the research, such as insufficient in-depth analysis on the mechanism controlling the increase in gas production. Therefore, in this study, the pretreatment methods of crushing and ball milling were used to treat lignite to analyze the mechanism that stimulates gas production. After the treatment, the lignite was subjected to microbial degradation and gas production experiment. The primary contributions of this research were an examination of structural differences between lignite processed using the two methods, a discussion of the factors both external and internal to the coal-to-methane conversion, and the provision of reference results for the development of coal biogasification pretreatment technology. Our research has substantial theoretical and practical implications for the exploration and development of coalbed methane resources because it can provide the groundwork for a better understanding of the biogas generation mechanism of coal seams and subsurface microbial gasification mining of coal.

2. Material and methods

2.1. Sample preparation

2.1.1. Coal samples

The samples of Shengli lignite were collected in the Ximeng region of China's Inner Mongolia Autonomous Region. The samples were sealed in aluminium foil bags right after collection, transferred to the lab, and stored in a dryer. Proximate analysis and ultimate analysis were used to determine the lignite's chemical composition. Table 1 displays the findings, indicating that the degree of coalification and ash content of the samples were low, and the volatile yield was high, implying the high potential of Shengli lignite for biodegradation.

Coal powder of varying particle sizes was used in the gas generation experiment. The lignite samples were crushed for 3min with a GS-2D pulverized coal crusher (HeBiShi XianFeng instrument and instrument company Limited) to form coal powder, which was then passed through a standard screen to obtain five particle size ranges: 100−200, 200−300, 300−400, 400−500, and greater than 500 mesh. The pulverized coal treated by ball milling was obtained using a QM-3SP4 planetary ball milling (Nanda Instrument). The sample was added to a ball mill tank made of polytetrafluoron and treated for 3 h with a speed of 400r/min at a ratio of 1:10(w: w) to stainless steel balls; these samples were then sized using a standard screen according to the same size ranges as those from the gas production pretreatment method.

2.1.2. Microbial community

The experimental flora, which was a high-efficiency exogenous flora that can degrade lignite to produce methane through enrichment and domestication, was obtained from sludge. The composition of the culture medium and methods of enrichment and domestication reference our previous work [21].

2.2. Experiment of biogenic gas production from coal

All experimental procedures on microbial degradation of lignite were carried out under the same controlled external conditions described below. A 100 mL anaerobic bottle was used as a reactor in the lignite biogas simulation experiment. Under sterile conditions, we put 50 mL of culture medium, 2 g of coal, and 5 mL of an experimental microbial community into the reactor. Air was removed from the reactor using an evacuating equipment and filled with high purity nitrogen to ensure an oxygen-free reaction environment. Biogenic gas from coal was produced in an experiment conducted at 37 °C and a pH of seven. The total gas output was obtained using the Draining Water Gathering Gas Technique. Gas samples were collected regularly to determine the gas production and composition. The calibration is controlled to ±0.1 m Under the same experimental conditions, three parallel samples were taken to ensure the accuracy of the experimental results. The data results in the manuscript were the mean values of three parallel sample test results, and error bars were added in the data graph to facilitate accurate analysis results [21].

Table 1
Proximate and ultimate analysis of lignite.

Proximate analysis		Ultimate analysis	
Moisture wt%	15.96	Hydrogen wt%	2.62
Ash wt%	9.08	Carbon wt%	50.96
Volatile wt%	43.97	Nitrogen wt%	0.72
Fixed carbon wt%	42.81	Sulfur wt%	0.19
Total sulfur wt%	0.25	Oxygen wt%	19.93

2.3. Analytical studies

2.3.1. Gas composition determination

Gas chromatography was used to analyze the gases and determine their components. Gas chromatography using a thermal conductivity detector (TCD) connected to PeakSimple Chromatography software was used to track methane generation. Manual injection, oven temperature of 60 °C, injector temperature of 120 °C, TCD temperature of 130 °C, and carrier gas pressure of 0.04 MPa were employed in conjunction with a PorpakN packed stainless steel column and ultra-high quality helium carrier gas for the separation [21].

2.3.2. Analysis via X-ray diffraction

The lignite was evaluated before and after pretreatment using an X-ray diffraction (XRD) spectrometer (SmartLab 9 KW) manufactured by the Neishu Company in Japan. The test was carried out at a scanning range of 5–80° and speed of 5°/min.

2.3.3. Fourier transform infrared spectroscopy analysis

Fourier transform infrared spectroscopy (FTIR; Nexus 670) was used to record the spectra of the lignite samples, with a resolution of 4 cm^{-1} in the area of 4000–400 cm^{-1}. After subtracting water and carbon dioxide interference, the total number of scans was 36. The resulting infrared spectrum's spectral peaks were divided using the curve fitting method, and the peak area was then calculated to accurately better properly reflect the infrared spectrum's variable characteristics.

In infrared testing, sample thickness and measurement time may affect the peak strength, therefore, to reduce the influence, the peak strength ratio (peak area ratio or peak height ratio) could be used to characterize the structural composition characteristics and changes. In this study, the peak area data obtained through peak fitting was used for quantitative analysis. The following three infrared spectral parameters (calculated with Eqs. (1)–(3)) were selected to characterize the microstructure of lignite:

$$I_1 = A_{2924}/A_{2964} \tag{1}$$

$$I_2 = A_{1703+1745}/A_{1618} \tag{2}$$

$$I_3 = A_{1618}/A_{1703+1618} \tag{3}$$

where, I_1 is the degree of the aliphatic chain length and branching (higher values indicate longer aliphatic chains and lower values indicate shorter side chains); I_2 represents the ratio of oxygen-containing functional groups to aromatic hydrocarbons; and I_3 represents the degree of maturation of organic matter [22].

2.3.4. Flammability testing

The pretreated coal samples were dried at 60 °C for 4 h and then tested for flammability testing with an STA409 Jupiter type Synchronous thermal analyzer (Netzsch Ltd., Germany). The combustion atmosphere was the simulated air, heated from room temperature to 800 °C at a heating rate of 10 °C/min. The carrier gas was argon, and the gas flow rate was 100 mL/min.

There are four distinct phases to the combustion of lignite: stage one (moisture release); stage two (volatile combustion); stage three (residual coke combustion), and finally stage IV (burnout) [23]. The samples' ignition temperatures were measured via thermogravimetry-derivative thermogravimetry (TG-DTG) [24]. On the same graph, we see both the thermogravimetry (TG) and the derivative thermogravimetry (DTG) curves. DTG's first peak value "A" was used to draw a vertical line that met the TG curve at point "B", where a tangent to the TG curve was also drawn. The ignition temperature was found to be the temperature at which the tangent met the parallel line marking the onset of weight loss from the primary combustion process (point "C") (Fig. 4). Based on the measured data of pure carbon, this test introduced the discriminant index R_w to characterize and calculated the combustion stability of coal samples according to the following Eq. (4):

$$Rw = \frac{655}{Ti} \times \frac{763}{Tp} \times \frac{(dw/dt)\max}{0.00582} = 8.5875 \times 10^7 \times \frac{(dw/dt)\max}{TiTp} \tag{4}$$

where Ti is the ignition temperature of coal sample in °C and Tp is the temperature corresponding to the maximum combustion weight loss rate of coal sample in °C; 655 is the temperature at which carbon will ignite; 763 is the temperature at which the rate of carbon combustion will peak; 0.00582 is the maximum loss rate of carbon combustion in s-1; Coal sample S^{-1} has a maximum weight loss rate of (dw/dt) max, where S^{-1} is the sample size.

2.3.5. Raman analysis

Micro-Raman Spectroscopy (in Via microscope) was used to acquire Raman spectra of lignite samples in the 400–4000 cm^{-1} range. Laser power is 0.3 mW, and the excitation light source wavelength is 532 nm. The scan count was 50, and the exposure time was 3 s. The Raman spectra of the 800−2000 cm^{-1} band were processed using the Origin 9.0 software.

3. Results and discussion

3.1. Characterization of gas production

The gas products were sampled after the lignite microbial degradation experiment ran for 15 days and analyzed subjectively qualitatively and quantitatively. Fig. 1 displays the outcomes of microbial breakdown of lignite over particle size ranges following the two treatments, which shows that the gas production contains two gases: methane and carbon dioxide, and the degradation gas production results of lignite with different particle sizes are different. Initially, the gas production increases with increasing particle size range to a maximum value and then decreased with increasing particle size range. The coal samples after the two treatment methods show the same gas production law in different particle size range. As the particle size range decreased, the degree of surface fragmentation of lignite increases; the smaller the particles of lignite, the higher the degradation rate and gas production of methanogens. On the other hand, lignite particles in the medium with smaller particle size ranges may agglomerate, reducing the contact surface between bacteria and lignite particles and, consequently, gas generation. In conclusion, the degradation of lignite under different treatment methods induced the highest gas production within the same particle size range (400−500 mesh).

After pretreatment with crushing and ball milling, the highest gas production after microbial degradation of lignite reached 39.90 mL and 50.90 mL, respectively, in which the methane content was 21.00 mL and 28.87 mL (Fig. 1(a and b)). The comparison results of two pretreatments in the five particle size ranges are presented in Fig. 1(c), in which the gas production after ball milling was higher than that after crushing, which had nothing to do with particle size. Raw coal and microbial flora were both held constant throughout all trials to ensure consistency. Each experiment had three parallel samples to reduce the influence of error. However, the biogas results of lignite after ball milling treatment were better after microbial degradation, which was more conducive to the utilization of microorganisms. It has been hypothesized that the structure of lignite had been changed. Therefore, the coal samples after different pretreatments were characterized to determine if the treatments caused structural changes to the lignite.

3.2. X-ray diffraction analysis

The XRD spectra of the lignite samples that were crushed and ball milled are displayed in Fig. 2(a). The characteristic peaks of the treated samples were essentially the same, among which, the presence of extremely disordered amorphous carbon elements in the coal samples was evidenced by the evident and highly intense diffraction peaks of kaolinite and quartz. There were two pronounced peaks at the 002 and 100 diffraction peak band, with diffraction angles of 26° and 47°, respectively. Diffraction peaks for aromatic microcrystalline structure (002 band) and fatty carbon microcrystalline structure (γ band) were observed. Comparatively, there were minimal difference in the peak type, area and height between the two pretreated coal samples. The crystalline structure of the coal samples was barely affected by the pretreatment procedures, while the coal samples after ball milling are more easily degraded with microorganisms, and the biogas yield was higher than that of the other one. Therefore, it was speculated that there were differences in functional groups or some structures between the two coal samples.

3.3. Fourier transform infrared spectroscopy analysis

3.3.1. Peak fitting of infrared spectra of coal

Generation of spectral peak superposition at certain positions in the infrared spectrum is relatively easy; determining the location and boundary of absorption peaks is challenging due to the presence of absorption bands from numerous functional groups in coal. Sample FTIR spectra are displayed in Fig. 2(b). Spectral lines between 3600 and 3000 cm^{-1} have been attributed to coal's primary functional groups—hydroxyl, aliphatic, and oxygen-containing—in prior research [25]. The analysis of the abovementioned functional groups is discussed below.

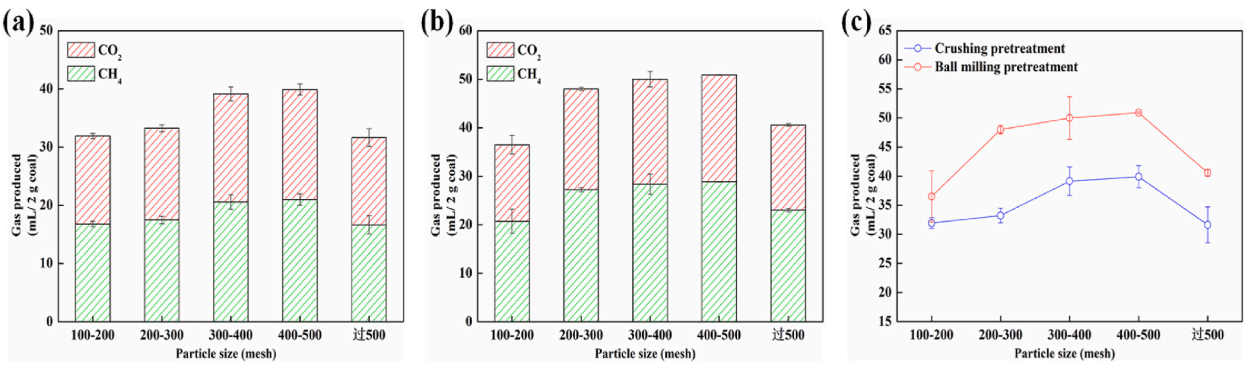

Fig. 1. Total gas production of the lignite biodegradation at different particle size range. (a) Crushing pretreatment; (b) Ball milling pretreatment; (c) Comparison of two treatments with same particle size range.

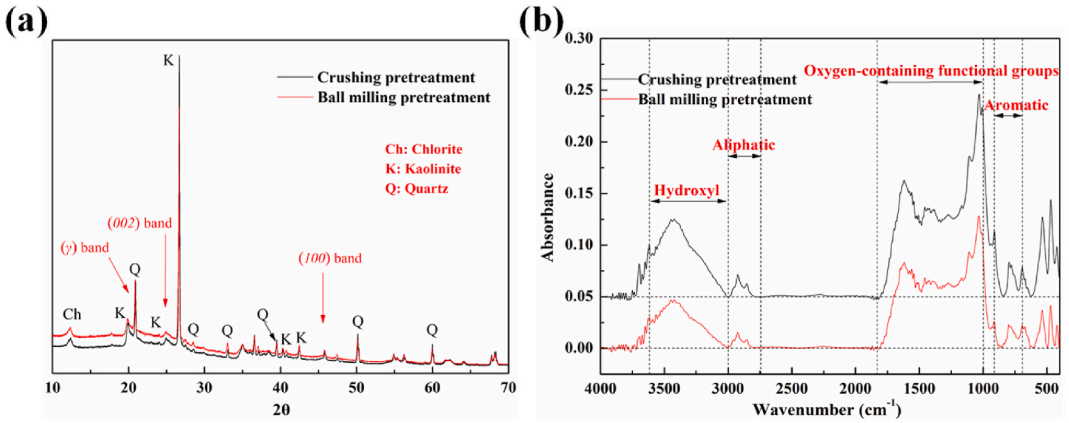

Fig. 2. XRD spectra and FTIR spectra of samples. (a) XRD spectra; (b) FTIR spectra.

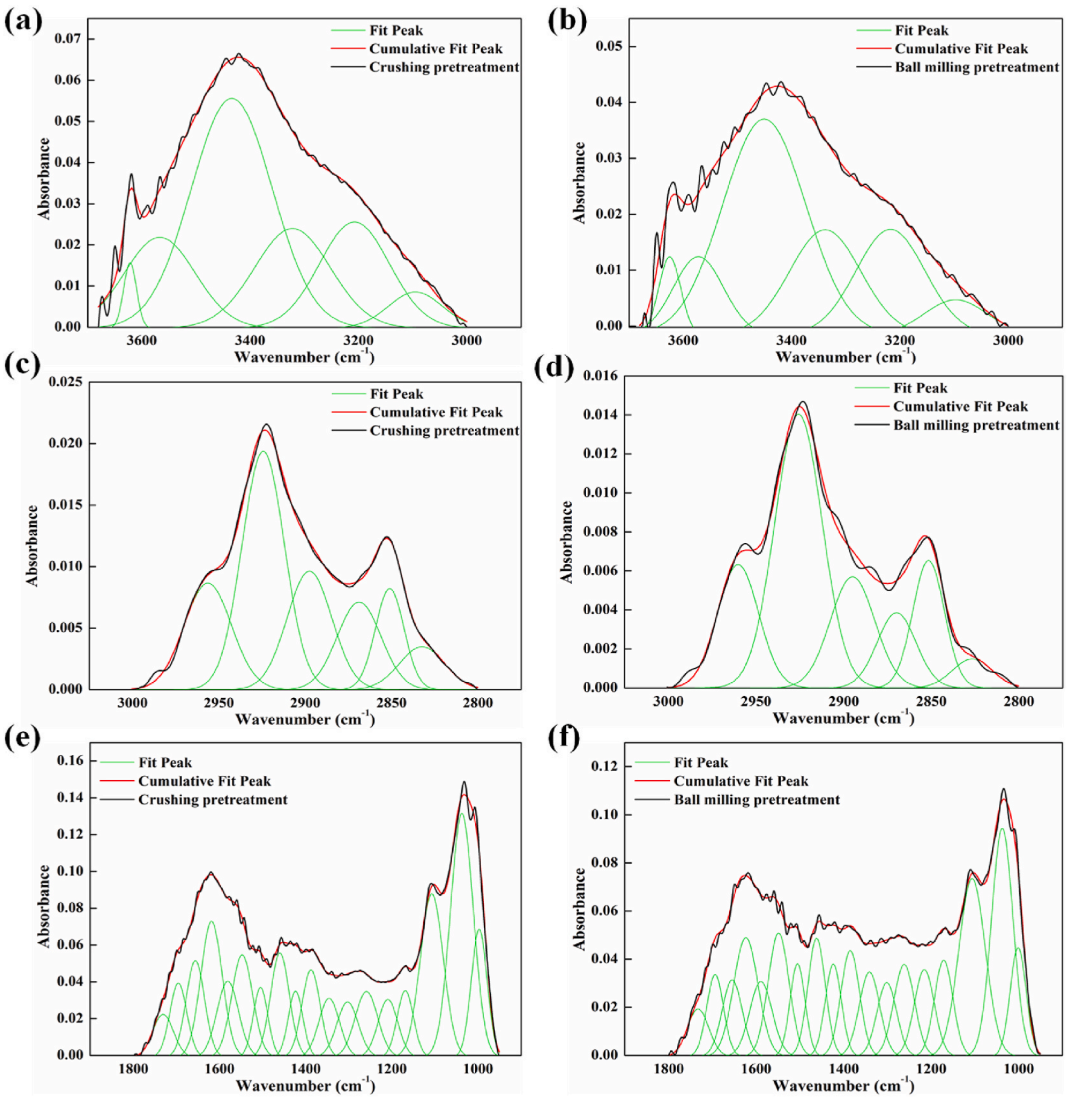

Fig. 3. FTIR spectra fitting curve of samples in different wavenumber ranges. (a, b) 3600−3000 cm^{-1}; (c, d) 3000−2800 cm^{-1}; (e, f) 1800−1000 cm^{-1}.

3.3.1.1. Spectral peak fitting of hydroxyl groups. The hydroxyl group on coal molecules was the most important for forming hydrogen bonds in the absorption vibration region, with wavenumber 3000–3600 cm^{-1}. The hydroxyl group may establish several different types of hydrogen bonds with various hydrogen bond receptors. The baseline corrected FTIR diagram revealed a significant spike near the wavenumber at 3620 cm^{-1}, which typically occurs when the steric hindrance cannot form hydrogen bonds or the hydrogen bonds formed are very weak; most scholars ascribe this peak to the vibration of free hydroxyl in coal [26], while others ascribe it to water (water of crystallization) in clay minerals (kaolin) [27]. Considering lignite's high ash content, the researchers hypothesized that the peak around the wavenumber at 3620 cm^{-1} was due to water in the silicate minerals. Coal molecules' primary functional group for forming hydrogen bonds was the hydroxyl group, which may form several hydrogen bond types with various hydrogen bond receptors. According to the classification of hydrogen bonds formed by hydroxyl groups in coal [26], the spectrum of this region includes six types: free hydroxyl hydrogen bonds (3620 cm^{-1}); hydrogen bonds (3560 cm^{-1}), with π electrons on an aromatic ring (OH-π); hydrogen bonds formed by self-associating hydroxyl groups (near 3428 cm^{-1}); oxygen-hydrogen bonds occurring in OH-ether formed from the interaction with ether (near 3300 cm^{-1}); hydrogen bonds forming ring structure (near 3218 cm^{-1}); and OH–N bonds (near 3098 cm^{-1}) [28]. Six Gaussian peaks were selected for fitting according to the above classification. The results of the peak fitting were displayed in Fig. 3(a,b). As a result of its low degree of coalification and high concentration of oxygen-containing functional groups, lignite is particularly susceptible to the influence of hydrogen bonding of various types. These properties enable methanogenic bacteria to more effectively use lignite to produce methane. The peak fitting results indicated that the self-associating hydroxyl group hydrogen bond contributed the most to the total hydrogen bond concentration in coal.

3.3.1.2. Spectral peak fitting of aliphatic hydrocarbons. Coal's infrared spectrum was observed to lie in the region of 3000–2800 cm^{-1}, which corresponds to the aliphatic C–H bond absorption vibration zone. Baseline correction of the FTIR figure (Fig. 2(b)) reveals two major peaks at around 2855 and 2925 cm^{-1}, which were attributed to the symmetric and antisymmetric stretching vibration of the saturated hydrocarbon methylene, respectively [27]. The symmetric stretching vibration of methyl groups attached directly to oxygen atoms was shown to be responsible for the peaks at 2871 and 2955 cm^{-1} wavenumbers [29], whereas the antisymmetric stretching vibration of methyl groups was found to be responsible for the shoulder peak at 2825 cm^{-1}. Additionally, the stretching vibration of methylidyne was linked to a peak location about 2890 cm^{-1} within the spectrum of symmetric and antisymmetric stretching vibration of methylene. As a result, six Gaussian peaks were chosen for fitting from this area, and the outcomes are depicted in Fig. (c) and (d). According to the data, aliphatic hydrocarbons predominated as long chains with few side chains in the treated lignite, which had more methylene and less methyl and methylidyne.

3.3.1.3. Spectral peak fitting of oxygen-containing functional groups. Coal's oxygen-containing functional groups mostly consist of hydroxyl, carboxyl, carbonyl, and ether oxygen, with hydroxyl groups having already been studied in Section 3.3.1.1. The other three types were distributed in the wavenumber region of 1800–1000 cm^{-1}; this regional spectrum is relatively complex as it also includes deformation vibration of methyl and methylene and stretching vibration of aromatic carbon-carbon double bond. For this purpose, peak fitting was performed on a set of 18 Gaussian peaks [22], and the results are displayed in Fig. 3(e) and (f). The C–O–C stretching vibration in Ar-O-C and Ar-O-Ar was shown to be responsible for the peak at 1034 cm^{-1} in the spectral distribution. It was determined that the 1200 cm^{-1} peak in the carbon oxygen bond stretching vibration was due to the stretching vibration of the phenolic hydroxyl group (C_6H_5–OH). The fundamental characteristic of lignite is the stretching vibration peak at 1700 cm^{-1}, which is due to the carboxylic acid functional group (-COOH). The carbonyl group stretching vibration peak occurred at 1340 cm^{-1}. Using acetic acid as substrate, methanogenic bacteria can convert it to methane by deoxymethylation. The existence of oxygen-containing functional groups in lignite is more conducive to the occurrence of microbial fermentation degradation process. The following parameter calculation proves this point.

3.3.2. Analysis of infrared structural parameters

Compared with the crushed lignite, the I_1 and I_2 values of lignite treated by ball milling increased significantly (Table 2), which

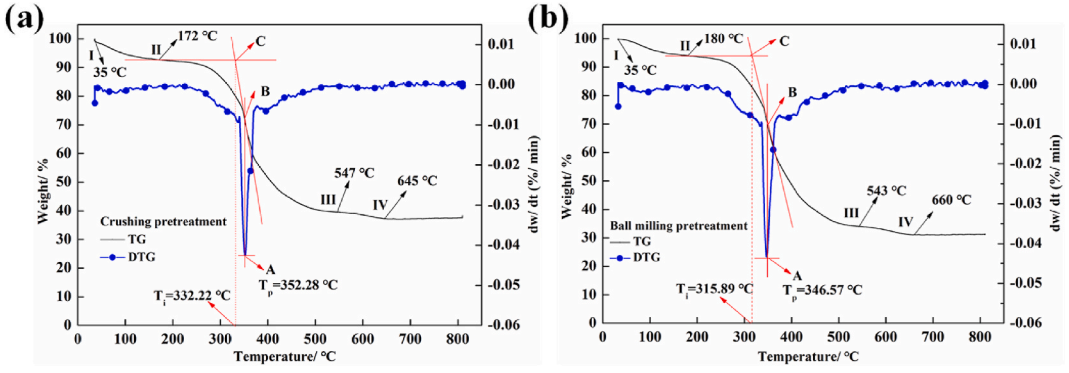

Fig. 4. TG and DTG curves of different coal samples. (a) crushing pretreatment; (b) ball milling pretreatment.

Table 2
FTIR parameters of coal samples.

Samples	A_{2924}	A_{2964}	A_{1703}	A_{1745}	A_{1618}	I_1	I_2	I_3
Crushing pretreatment	34.825	17.242	3.768	2.626	8.661	2.020	0.738	0.697
Ball milling pretreatment	42.703	16.339	3.604	2.661	7.661	2.614	0.818	0.680

could be attributed to three potential cases: an increase in the fatty chain or content of oxygen-containing functional groups, or a decreased in the aromatic hydrocarbons; the low carbonization of coal is more conducive to microbial degradation [30,31]; the I_3 was almost unchanged, indicating that there was an elevated levels of oxygen-containing functional groups when lignite was treated by ball milling; this provided a more conducive condition for biodegradation, and thus promoted gas production [32].

3.4. Flammability testing

Coal samples after both processes are treated and their TG and DTG curves are showed in Fig. (a,b) and combustion response characteristics are listed in Table 3. The ignition temperature was the most affected of the four stages of coal sample combustion, however there was no statistically significant difference between the two treatment procedures. The lignite ignition point after ball milling treatment was 315.89 °C, which decreased by 4.92% compared that after crushing. The R_w of lignite after crushing was 3.117, while that of lignite after ball milling increased by 8.53%, indicating that ball milling was not conducive to the combustion stability of coal. As the ignition point is strongly related to the degree of coalification, the decreased ignition point after ball milling indicates that the degree of coalification was lower. Infrared study shows that when the amount of oxygen-containing functional groups in coal increases during oxidation, its ignition point drops. Having them on hand aids in the biodegradation of lignite by microorganisms and boosts biogas output.

3.5. Raman analysis

First-order Raman spectra for highly soluble carbon compounds like low-rank coal or coal coke were fitted with a 10-band Gaussian distribution [33]. Fig. 5(a,b) shows that the majority of the 10 fitting peaks occurred at 1540 cm^{-1} (GR), 1465 cm^{-1} (V), and 1380 cm^{-1} (VR), all of which are characteristic of methylene or methyl structures, in particular those containing a small aromatic ring. Furthermore, aromatic ring vibration was found to be more responsible for the G-peak band [34]. C–C bonds inside aromatic rings, especially those with more than six rings but fewer than the number of carbon atoms in graphite, were found to be primarily responsible for the D-peak band. In addition, the coal structure was responsible for the appearance of spectral lines at 1700 (GL), 1230 (SL), 1185 (S), 1060 (SR), and 960 (R) cm^{-1}.

The Raman spectra of carboniferous materials had two noticeable peaks: the D-peak (1327−1360 cm^{-1}) and G-peak (1550−1598 cm^{-1}). D-peak refers to planar defects or disordered structures between infrastructural units [35]. The G-peak arises from the aromatic ring of aromatic carbonaceous materials, which forms the ordered structure. As shown in Table 4, the D-peak and G-peak intensities of ball-milled coal samples were lower than those of crushed coal samples. This happened because the ball milling operation used up some of the carbon sources. A reduction in the lignite ratio (I_D/I_G) after ball milling generally leads to an increase in the ordered structure. In the process of ball milling, more refers to the disordered structure represented by the D-peak is stripped. Although the ordered structure represented by G-peak consumed, it consumed to a lesser degree, which was indicated by the slight increase in the peak height, indicating that it is difficult to alter the ordered structure of lignite. Corresponding to biogas production from microbial degradation of the two types of lignite, the increase in the disordered structure promoted the biodegradation and subsequent biogas production.

The usual structure of amorphous carbon materials is represented by the peaks labelled GR, VL, and VR between the D-peak and the G-peak. Specifically, it alludes to the compact aromatic ring complexes that have between three and five condensed rings [33]. An easy way to quantify the huge aromatic ring system and aromatic rings often present in amorphous carbon is to compare the ratio of the highest peak of the D-peak to the sum of the peak heights of the three peaks. Table 5 reveals shows that after ball milling, the structure of small aromatic rings in lignite increased, while the structure of large aromatic rings decreased. The ball milling treatment caused the disordered structure to become increasingly unstable, which was conducive to the degradation of lignite by microbial flora, thus promoting gas production. It also corresponds to the gas production after ball milling was higher than that after crushing treatment in the previous test.

Table 3
Combustion performance parameters of coal samples.

Samples	T_i (°C)	T_p (°C)	(dw/dt) max (S^{-1})	R_w
Crushing pretreatment	332.22	352.28	0.04248	3.117
Ball milling pretreatment	315.89	346.57	0.04313	3.383

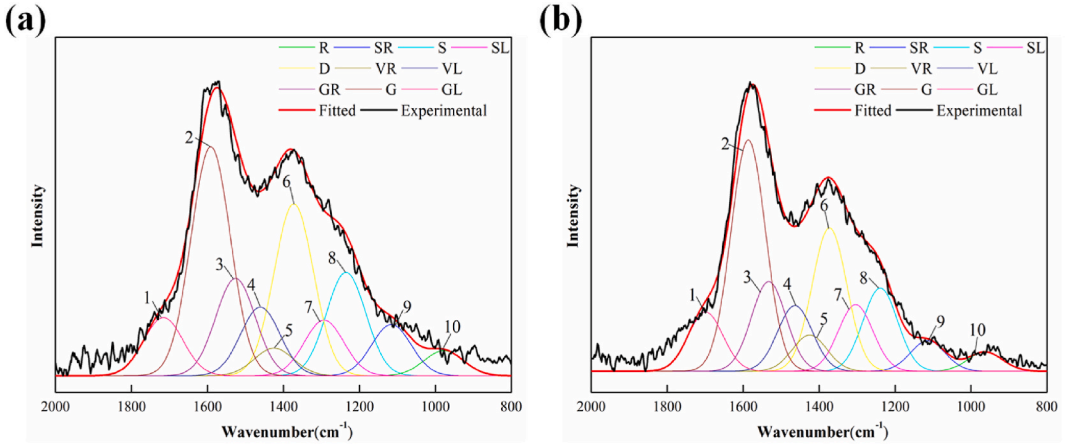

Fig. 5. Raman spectra fitting curve of samples. (a) Crushing pretreatment; (b) Ball milling pretreatment.

Table 4
Raman fitting data of coal samples.

Samples	D-peak		G-peak		I_D/I_G(A)
	Max height	Area intg	Max height	Area intg	
Crushing pretreatment	6288.13	816502.82	8382.90	1088504.54	0.75
Ball milling pretreatment	5246.74	598388.43	8463.04	965206.30	0.62

Table 5
Raman fitting data of coal samples.

Max height	D	G_R	V_L	V_R	specific value
Crushing pretreatment	6288.13	3562.07	2508.53	1008.17	0.89
Ball milling pretreatment	5246.74	3281.22	2400.34	1318.84	0.75

3.6. Microbial community analysis

The results of diversity analysis of the microbial community are shown in Fig. 6, showing the structure of microbial communities from kingdom, phylum, order, and genus, respectively. Fig. 6(a) shows the microbial diversity and distribution in sample at the kingdom level. The microbial community composition was dominated by bacteria, whose relative abundance was 95%, much higher than that of archaea (4%). The flora was taxonomically attributed to 13 phyla in addition to unclassified and other phyla (<0.4%). The core bacteria were *Firmicutes*, *Bacteroidetes*, and *Proteobacteria*, the core of archaea was *Euryarchaeota*; the sum of the abundance of core bacteria accounted for more than 80%.

Fig. 6(c) shows the microflora at the order classification level in the degradation process. *Clostridiales* and *Bacteroidales* accounted for more than 45% and had an important position. *Methanosarcinales* were methanogens detected at the level. *Methanosarcinales* produced methane by decomposing acetic acid and consuming hydrogen as the main metabolic pathways. Methane was mainly produced by metabolizing formate, alcohol, and carbon dioxide under the action of *Methanosarcinales* [36]. Twenty-three genera were identified in addition to unclassified and other genera (<0.5%) (Fig. 6(d)). The core genera were acidogenic bacteria that could metabolize organic matter, among which *Bacteroides* could degrade nitrogenous heterocyclic macromolecules such as pyridine and indoles to form low weight molecule organic acids and alcohols. Formate dehydrogenase produced in cells of some genera decomposed formic acid into carbon dioxide and hydrogen [37–39]. Some strains of *Clostridium* used carbon dioxide to produce acid [40] and their existence confirmed the source of carbon dioxide in the gas production. *Sedimentibacter* fermented amino acids to produce acetic acid and butyric acid, and other bacteria could convert 4-hydroxybenzoic acid and 3, 4-dicarboxylic acid into phenol and catechol by reversible dihydroxylation [41]. The archaea were primarily *Methanocorpusculum* and *Methanosarcina*, which played an important role and were the main functional bacteria that produce methane. The former accounted for approximately 97% of the archaea and was the dominant flora, it could form methane in three ways [42,43]. After several passages, the biogas degradation of lignite by microbial flora is relatively stable, and the number of methanogens in the flora is always changing [44]. In this study, *Methanosarcina* is the dominant bacterium, which may be because it has a self-protection mechanism through exopolysaccharide, thus possessing a certain tolerance to adversity and less affected [45,46]. In the biodegradation process of lignite, there was a synergistic effect among microbial communities, and some microbiota can utilize metabolites from each other. The biodegradation of lignite is a progressive process. Therefore, the structure destruction pretreatment of lignite is conducive to its utilization by microorganisms.

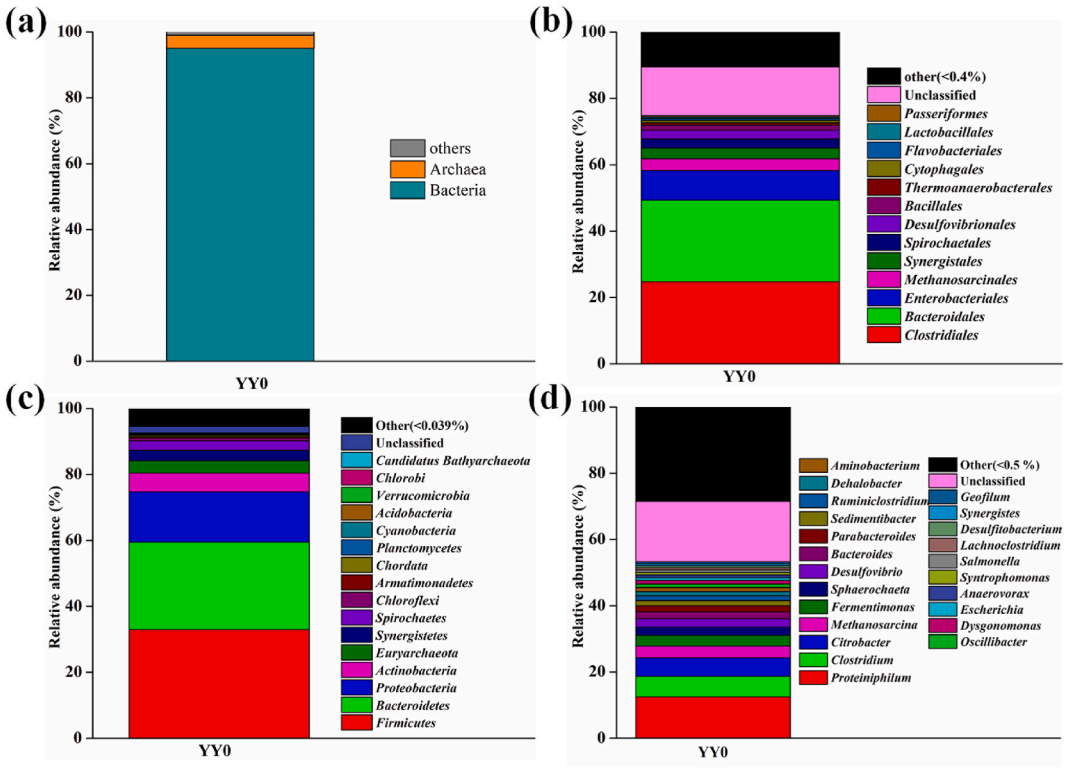

Fig. 6. Microbial diversity and distribution in sample at the kingdom, phylum, order, and genus level. (a) kingdom; (b) phylum; (c) order; (d) genus.

4. Conclusions

For the lignite treated by crushing and ball milling, the gas production after microbial degradation was found to be related to the particle size. The gas production reaches the highest at 400−500 mesh, and the biogas (methane) reaches 21.00, 28.87 mL/2 g lignite respectively. The structure of lignite after the two treatments was different. The increase in oxygen-containing functional groups and small aromatic ring structures in the lignite after the ball milling treatment leads to instability of the lignite structure and decrease in the coalification degree, which was conducive to the degradation and utilization of lignite by microorganisms. Therefore, the biogas production of lignite was improved under these pretreatment methods. The pretreatment of lignite can promote its degradation by microbial flora via destroying the structure of lignite. Some basic analyses conducted in this study provides reference data for future research of the degradation mechanism and to promote new ideas of microbial degradation of lignite.

CRediT authorship contribution statement

Lin Yang: Investigation, Writing-Original Draft, Software. **Yongfeng Zhang:** Supervision, Funding acquisition. **Zhifei Hao:** Writing-Review & Editing, Visualization. **Junying Zhang:** Conceptualization.

Declaration of competing interest

The authors declare that they have no known competing financial interests or personal relationships that could have appeared to influence the work reported in this paper

Acknowledgments

The authors would like to gratefully acknowledge the financial support provided by the National Natural Science Foundation Project of China (22206090), and Natural Science Foundation Project of Inner Mongolia Autonomous Region (2018LH02010 and 2022QN02009).

References

[1] K. Hagos, J.P. Zong, D.X. Li, C. Liu, X.H. Lu, Anaerobic co-digestion process for biogas production: progress, challenges and perspectives, Renewable Sustainable Energy Rev. 76 (2017) 1485–1496, https://doi.org/10.1016/j.rser.2016.11.184.

[2] X.B. Su, W.Z. Zhao, D.P. Xia, The diversity of hydrogen-producing bacteria and methanogens within an in situ coal seam, Biotechnol. Biofuels 11 (2018) 245, https://doi.org/10.1186/s13068-018-1237-2.

[3] B.Y. Wang, C. Tai, L. Wu, L.Y. Chen, J.M. Liu, B. Hu, D.y. Song, Methane production from lignite through the combined effects of exogenous aerobic and anaerobic microflora, Int. J. Coal Geol. 173 (2017) 84–93, https://doi.org/10.1016/j.coal.2017.02.012.

[4] H. Zheng, T.Y. Chen, V. Rudolph, S.D. Golding, Biogenic methane production from Bowen Basin coal waste materials, Int. J. Coal Geol. 169 (2017) 22–27, https://doi.org/10.1016/j.coal.2016.09.006.

[5] A. Scott, W. Kaiser, W. Ayers, Thermogenic and secondary biogenic gases, San-Juan Basin, Colorado and New-Mexico-implications for coalbed gas producibility, Am. Assoc. Petrol. Geol. Bull. 78 (1994) 1186–1209, https://doi.org/10.1029/94GL00698.

[6] H. Chen, Y. Qin, Z. Deng, M. Geng, G.Z. Li, G.J. Sang, D.P. Xia, Factors influencing biogenic gas production of low-rank coal beds in the Jiergalangtu Sag, Erlian Basin. Nat. Gas Ind. 6 (2019) 1–6, https://doi.org/10.1016/j.ngib.2019.01.001.

[7] B.B. Wang, Z.S. Yu, Y.M. Zhang, H.X. Zhang, Microbial communities from the Huaibei Coalfield alter the physicochemical properties of coal in methanogenic bioconversion, Int. J. Coal Geol. 202 (2019) 85–94, https://doi.org/10.1016/j.coal.2018.12.004.

[8] W.H. Orem, M.A. Voytek, E.J. Jones, H.E. Lerch, A.L. Bates, M.D. Corum, P.D. Warwick, A.C. Clark, Organic intermediates in the anaerobic biodegradation of coal to methane under laboratory conditions, Org. Geochem. 41 (2010) 997–1000, https://doi.org/10.1016/j.orggeochem.2010.03.005.

[9] P. Gupta, A. Gupta, Biogas production from coal via anaerobic fermentation, Fuel 118 (2014) 238–242, https://doi.org/10.1016/j.fuel.2013.10.075.

[10] D. Mayumi, H. Mochimaru, H. Tamaki, K. Yamamoto, H. Yoshioka, Y. Suzuki, Y. Kamagata, S. Sakata, Methane production from coal by a single methanogen, Science 354 (2016) 117–122, https://doi.org/10.1126/science.aaf8821.

[11] H. Wang, H. Lin, C.P. Rosewarne, D. Li, S. Gong, P. Hendry, P. Greenfield, N. Sherwood, D.J. Midgley, Enhancing biogenic methane generation from a brown coal by combining different microbial communities, Int. J. Coal Geol. 154–155 (2016) 107–110, https://doi.org/10.1016/j.coal.2015.12.006.

[12] S.R. Haq, S. Tamamura, T. Igarashi, K. Kaneko, Characterization of organic substances in lignite before and after hydrogen peroxide treatment: implications for microbially enhanced coalbed methane, Int. J. Coal Geol. 185 (2018) 1–11, https://doi.org/10.1016/j.coal.2017.11.009.

[13] K. Jian, G. Chen, C. Guo, G.S. Ma, Z.L. Ru, Biogenic gas simulation of low-rank coal and its structure evolution, J. Pet. Sci. Eng. 173 (2019) 1284–1288, https://doi.org/10.1016/j.petrol.2018.11.005.

[14] P. Shao, A.K. Wang, W.F. Wang, Experimental simulation of biogenic coalbed gas generation from lignite and high-volatile bituminous coals, Fuel 219 (2018) 111–119, https://doi.org/10.1016/j.fuel.2018.01.087.

[15] M.A. Sabar, M.I. Ali, N. Fatima, A.Y. Malik, A. Jamal, M. Farman, Z. Huang, M. Urynowicz, Degradation of low rank coal by Rhizopus oryzae isolated from a Pakistani coal mine and its enhanced releases of organic substances, Fuel 253 (2019) 257–265, https://doi.org/10.1016/j.fuel.2019.04.101.

[16] S. Ghosh, P. Jha, A.S. Vidyarthi, Unraveling the microbial interactions in coal organic fermentation for generation of methane — a classical to metagenomic approach, Int. J. Coal Geol. 125 (2014) 36–44, https://doi.org/10.1016/j.coal.2014.02.005.

[17] W.Z. Zhao, X.B. Su, D.P. Xia, D. Li, H.Y. Guo, Contribution of microbial acclimation to lignite biomethanization, Energy Fuels 34 (2020) 3223–3238, https://doi.org/10.1021/acs.energyfuels.9b03137.

[18] R. Haider, M.A. Ghauri, J.R. SanFilipo, E.J. Jones, W.H. Orem, C.A. Tatu, K. Akhtar, N. Akhtar, Fungal degradation of coal as a pretreatment for methane production, Fuel 104 (2013) 717–725, https://doi.org/10.1016/j.fuel.2012.05.015.

[19] L. Wu, H.Z. Li, B. Cao, T.Q. Zhao, Z.H. Wang, Study on gas characterization and fluorescence characteristics of intermediates in biogenic gas production from lignite by ultrasound assisted hydrogen peroxide pretreatment, Arabian J. Geosci. 14 (2021), https://doi.org/10.1007/s12517-021-06676-5.

[20] Q.R. Wang, H.G. Guo, H.J. Wang, M.A. Urynowicz, A.Y. Hu, C.P. Yu, P. Fallgren, S. Jin, H. Zheng, R.J. Zeng, F.J. Liu, B. Chen, R.G. Zhang, Z.X. Huang, Enhanced production of secondary biogenic coalbed natural gas from a subbituminous coal treated by hydrogen peroxide and its geochemical and microbiological analyses, Fuel 236 (2019) 1345–1355, https://doi.org/10.1016/j.fuel.2018.09.114.

[21] L. Yang, Y.F. Zhang, Z.F. Hao, D.Q. Ding, Z.Y. Liu, Clean utilization of lignite to produce biomethane by optimizing the microbial community, Energy 262 (2023), 125533, https://doi.org/10.1016/j.energy.2022.125533.

[22] J. Ibarra, E. Muñoz, R. Moliner, FTIR study of the evolution of coal structure during the coalification process, Org. Geochem. 24 (1996) 725–735, https://doi.org/10.1016/0146-6380(96)00063-0.

[23] H.Y. Guo, S.F. Zhao, D.P. Xia, L. Wang, J.H. Lv, H.F. Yu, X.J. Jiao, Efficient utilization of coal slime using anaerobic fermentation technology, Bioresour. Technol. 332 (2021), 125072, https://doi.org/10.1016/j.biortech.2021.125072.

[24] X.Y. Huang, X.M. Jiang, X.X. Han, H. Wang, Combustion characteristics of fine- and micro-pulverized coal in the Mixture of O2/CO2, Energy Fuels 22 (2008) 3756–3762, https://doi.org/10.1021/ef800444c.

[25] D. Wu, H. Zhang, G. Hu, W. Zhang, Fine characterization of the macromolecular structure of Huainan coal using XRD, FTIR, C-13-CP/MAS NMR, SEM, and AFM techniques, Molecules 25 (2020) 2661, https://doi.org/10.3390/molecules25112661.

[26] P.C. Painter, M. Sobkowiak, J. Youtchefft, FT-IR study of hydrogen bonding in coal, Fuel 66 (1987) 973–978, https://doi.org/10.1016/0016-2361(87)90338-3.

[27] H. Machnikowska, A. Krztoń, J. Machnikowski, The characterization of coal macerals by diffuse reflectance infrared spectroscopy, Fuel 81 (2002) 245–252, https://doi.org/10.1016/s0016-2361(01)00125-9.

[28] A. Furmann, A. Schimmelmann, S.C. Brassell, M. Mastalerz, F. Picardal, Chemical compound classes supporting microbial methanogenesis in coal, Chem. Geol. 339 (2013) 226–241, https://doi.org/10.1016/j.chemgeo.2012.08.010.

[29] J.Y. Jiang, W.H. Yang, Y.P. Cheng, Z.D. Liu, Q. Zhang, K. Zhao, Molecular structure characterization of middle-high rank coal via XRD, Raman and FTIR spectroscopy: implications for coalification, Fuel 239 (2019) 559–572, https://doi.org/10.1016/j.fuel.2018.11.057.

[30] D. Ritter, D. Vinson, E. Barnhart, D.M. Akob, M.W. Fields, A.B. Cunningham, W. Orem, J.C. McIntosh, Enhanced microbial coalbed methane generation: a review of research, commercial activity, and remaining challenges, Int. J. Coal Geol. 146 (2015) 28–41, https://doi.org/10.1016/j.coal.2015.04.013.

[31] D. Mohanty, S. Chattaraj, A.K. Singh, Influence of coal composition and maturity on methane storage capacity of coals of Raniganj Coalfield, India, Int. J. Coal Geol. 196 (2018) 1–18, https://doi.org/10.1016/j.coal.2018.06.016.

[32] Z.X. Gao, H.Y. Guo, X.L. Liu, Q. Wang, J.H. Lv, S. Liu, H.F. Yu, X.J. Yin, Controlling mechanism of coal chemical structure on biological gas production characteristics, Int. J. Energy Res. 44 (2020) 5008–5016, https://doi.org/10.1002/er.5276.

[33] X.J. Li, J. Hayashi, C.Z. Li, FT-Raman spectroscopic study of the evolution of char structure during the pyrolysis of a Victorian brown coal, Fuel 85 (2006) 1700–1707, https://doi.org/10.1016/j.fuel.2006.03.008.

[34] J.Y. Jiang, S. Zhang, P. Longhurst, W.H. Yang, S.J. Zheng, Molecular structure characterization of bituminous coal in Northern China via XRD, Raman and FTIR spectroscopy, Spectrochim. Acta, Part A 255 (2021), 119724, https://doi.org/10.1016/j.saa.2021.119724.

[35] R. Morga, I. Jelonek, K. Kruszewska, W. Szulik, Relationships between quality of coals, resulting cokes, and micro-Raman spectral characteristics of these cokes, Int. J. Coal Geol. 144–145 (2015) 130–137, https://doi.org/10.1016/j.coal.2015.04.006.

[36] E.M. Ryan, D. Bartell, Sabrina Mueller-Spitz, T. Gregory, Kleinheinz investigation of Methanosarcinales and Methanomicrobiales presence within a dry anaerobic digester, J. Microbiol. Res. 5 (2015) 101–108, https://doi.org/10.5923/j.microbiology.20150503.04.

[37] A. Caro-Quintero, K.M. Ritalahti, K.D. Cusick, F.E. Löffler, K.T. Konstantinidis, D. Relman, The chimeric genome of sphaerochaeta: nonspiral spirochetes that break with the prevalent dogma in spirochete biology, mBio 3 (2012), https://doi.org/10.1128/mBio.00025-12.

[38] S. Kim, H. Jeong, J. Chun, Clostridium aestuarii sp. nov., from tidal flat sediment, Int. J. Syst. Evol. Microbiol. 57 (2007) 1315–1317, https://doi.org/10.1099/ijs.0.64428-0.

[39] K.M. Ritalahti, S.D. Justicia-Leon, K.D. Cusick, N. Ramos-Hernandez, M. Rubin, J. Dornbush, F.E. Loffler, Sphaerochaeta globosa gen. nov., sp nov. and Sphaerochaeta pleomorpha sp nov., free-living, spherical spirochaetes, Int. J. Syst. Evol. Microbiol. 62 (2012) 210–216, https://doi.org/10.1099/ijs.0.023986-0.

[40] H.M. Wexler, Bacteroides: the good, the bad, and the nitty-gritty, Clin. Microbiol. Rev. 20 (2007) 593–621, https://doi.org/10.1128/CMR.00008-07.

[41] H. Imachi, S. Sakai, T. Kubota, M. Miyazaki, Y. Saito, K. Takai, Sedimentibacter acidaminivorans sp. nov., an anaerobic, amino-acid-utilizing bacterium isolated from marine subsurface sediment, Int. J. Syst. Evol. Microbiol. 66 (2016) 1293–1300, https://doi.org/10.1099/ijsem.0.000878.

[42] J. De Vrieze, T. Hennebel, N. Boon, W. Verstraete Methanosarcina, The rediscovered methanogen for heavy duty biomethanation, Bioresour. Technol. 112 (2012) 1–9, https://doi.org/10.1016/j.biortech.2012.02.079.
[43] R.K. Thauer, A.K. Kaster, H. Seedorf, W. Buckel, R. Hedderich, Methanogenic archaea: ecologically relevant differences in energy conservation, Nat. Rev. Microbiol. 6 (2008) 579–591, https://doi.org/10.1038/nrmicro1931.
[44] M.S. Green, K.C. Flanegan, P.C. Gilcrease, Characterization of a methanogenic consortium enriched from a coalbed methane well in the Powder River Basin, U.S. A. Int. J. Coal Geol. 76 (2008) 34–45, https://doi.org/10.1016/j.coal.2008.05.001.
[45] K.L. Anderson, E.E. Apolinario, K.R. Sowers, Desiccation as a long-term survival mechanism for the archaeon Methanosarcina barkeri, Appl. Environ. Microbiol. 78 (2012) 1473–1479, https://doi.org/10.1128/AEM.06964-11.
[46] X. Qu, L. Mazeas, V.A. Vavilin, J. Epissard, M. Lemunier, J.M. Mouchel, P.J. He, T. Bouchez, Combined monitoring of changes in delta(CH_4)-C-13 and archaeal community structure during mesophilic methanization of municipal solid waste, FEMS Microbiol. Ecol. 68 (2009) 236–245, https://doi.org/10.1111/j.1574-6941.2009.00661.x.